A fracture mechanics model to study indentation cutting

Terzano, M.; Spagnoli, A.; Ståhle, P.

Published in:
Fatigue and Fracture of Engineering Materials and Structures

DOI:
10.1111/ffe.12750

2018

Document Version:
Early version, also known as pre-print

Received: 25 July 2017 | Revised: 9 October 2017 | Accepted: 11 November 2017

DOI: 10.1111/ffe.12750

SPECIAL ISSUE - IGF INTERNATIONAL-STRUCTURAL INTEGRITY

WILEY

A fracture mechanics model to study indentation cutting

M. Terzano[1] | A. Spagnoli[1] | P. Ståhle[2]

[1]Department of Engineering and Architecture, University of Parma, Parco Area delle Scienze, 181/A, 43124 Parma, Italy

[2]Division of Solid Mechanics, Lund University, SE-221 00 Lund, Sweden

Correspondence
A. Spagnoli, Department of Engineering and Architecture, University of Parma, Parco Area delle Scienze, 181/A, 43124 Parma, Italy.
Email: spagnoli@unipr.it

Abstract

Many cutting processes, such as chopping, slicing, and carving, consist in 2 different stages: an initial stage of indentation, in which the cutting tool is pushed into the material under the action of an external force, and a second stage, where the target material undergoes a progressive separation. This second stage is characterised by the formation of a fracture surface followed by the cut propagation due to the increasing external force, until eventually a steady state might occur. The purpose of this paper is to analyse the cutting process by means of some concepts of fracture mechanics and discuss the occurrence of the steady state. A simple model is used to obtain an analytic expression of the stress intensity factor at the tip of the cut and investigate the evolution of the fracture process. It is found that the cut propagation depends on the wedge sharpness. The analytic results are compared with finite element analyses, where the effect of tip blunting due to plasticity is taken into account. The influence of the cutting tool geometry is also discussed.

KEYWORDS

cutting, crack tip plasticity, fracture mechanics, sharpness

1 | INTRODUCTION

Separation of materials by means of a cutting tool is a commonplace process of several disciplines and applications. In the scientific literature, a great number of studies are available, most of them focusing on a single field and exploring the related issues with a specific material and cutting technique. A comprehensive survey on cutting applied to different materials can be found, for instance, in the book by Atkins.[1]

The mechanics of the cutting process has received a considerable attention in relation to the applications in metal machining, with several studies investigating the competing contributions of plasticity and friction.[2-4] The main focus was the process of chip formation occurring in the so-called orthogonal cutting. Commonly, this term has been used to describe the process of separation caused by a cutting tool along a surface parallel to the original surface of the target material (Figure 1A). Only in more recent research, Atkins[5,6] has established that the contribution from fracture terms must also be included in the analyses, and showed that the cutting forces depend on the fracture toughness of the target material. Exploiting the similarity of orthogonal cutting with the splitting of a cantilever

Nomenclature: a, Half length of the cut; a_1, Position of the separation point; a_2, Position of the point of displacements singularity; b, Plate thickness; COD, Crack opening displacement; $CTOD$, Crack tip opening displacement; E, Young elastic modulus; h, Shape of the elliptic wedge; h_o, Length of the ellipse minor semiaxis; $K_{I,a}$, Stress intensity factor at the tip of the cut; K_{I,a_1}, Stress intensity factor at the point a_1; K_{I,a_2}, Stress intensity factor at the point a_2; K_{Ic}, Fracture toughness of the material; K_R, Stress intensity factor for $\ell = a$; r_y, Irwin's plastic zone length; r_{yc}, Irwin's plastic zone length, when $K_{I,a} = K_{Ic}$; $r_{y,R}$, Irwin's plastic zone length, when $K_{I,a} = K_R$; R_c, Tip radius of the cut in critical conditions; R_t, Generic wedge tip radius; α, Wedge opening angle; θ, Wedge sharpness; σ_o, Uniform external pressure; σ_y, Contact normal stresses; σ_{ys}, Yield stress of the material; τ_{xy}, Contact shear stresses; ρ, Radius of curvature at the elliptic wedge tip; ℓ, Insertion length of the cutting tool

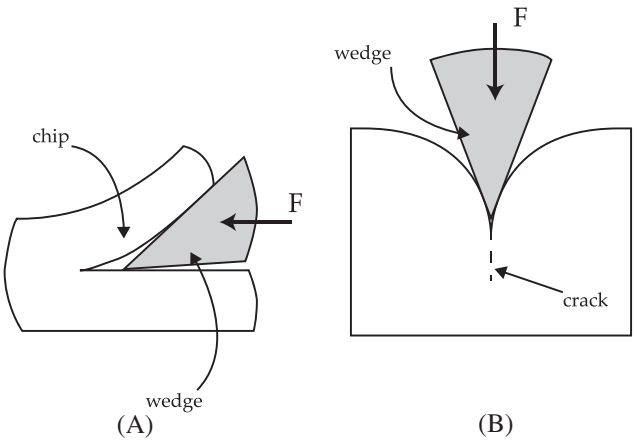

FIGURE 1 Schematic of two of the main cutting types. A, Orthogonal cutting. B, Indentation cutting. F is the cutting force

beam by means of a rigid wedge, Williams[7] and Williams et al[8] were able to obtain a complete picture of the contributions of friction, plasticity, and fracture toughness on the chip formation. An interesting aspect of their model is the occurrence of crack tip touching, when the force applied to the wedge is increased beyond a certain limit or the rake angle is decreased. Further contributions in the ultraprecision machining have also considered the influence of the cutting edge radius and the depth of the cut.[9,10]

Most of the previous concepts are central also in different cutting techniques, such as chopping, slicing, and carving. These are often described as examples of the indentation cutting, defined as a process in which the tool penetrates perpendicularly into the material, and cutting occurs along the line of symmetry of the tool[11] (Figure 1B). Indentation comprises an initial stage in which the tool is pushed through the target material under an applied load, generating a deformation that may consist of both elastic and plastic components. The indentation of ductile materials by means of a sharp rigid wedge was studied several years ago by Hill et al,[12] and more recently, an interesting work by Ciavarella et al[13] has provided an insight in the contact mechanics features of indentation. Specifically, it is pointed out how the singular state of stress implied by a sharp wedge does not exist in practice, because of the effect of edge rounding and plastic flow.

Following the initial indentation, a cut or crack initiates, and the blade continues to penetrate in the material with increasing force until steady-state cutting is established. Here, the behaviour is strongly affected by the sharpness of the cutting instrument. Sharpness is a key parameter in all cutting applications, since it has a direct effect on the cutting forces, the quality of the cut surface, and the life of the cutting instrument. An exhaustive definition of the blade sharpness was given by McCarthy et al,[14,15] through indentation experiments on elastomeric materials. Different contributions need to be considered if cutting is applied to soft materials, such as food or biological tissues, because of the non-linear mechanical behaviour, viscoelastic effects, and temperature dependence.[16,17]

The purpose of this paper is to investigate the quasi-static fracture stage of indentation cutting by means of a simple model, which can be handled analytically, and is applicable to the indentation cutting of a large class of materials, within the range of small scale yielding. The initial indentation stage is not considered here; instead, the focus is on the fracture process that follows, which is mainly influenced by the wedge sharpness. A definition of sharpness is obtained as the ratio between the wedge tip radius, the fracture toughness, and the modulus of elasticity of the target material. We have then used finite element analyses to account for the effect of local plasticity and explore the consequences of crack tip blunting on the fracture process. Different tool geometries have been explored throughout the analyses. This paper is divided in 2 main parts. In the first part, Section 2, after introducing the model used to describe the cutting process, we present the analytic solution and discuss the implications of the wedge sharpness on the fracture process. Here, the target material is elastic, and the cutting tool consists of a rigid elliptic wedge. The second part, Section 3, contains the results of the finite element analyses. First, we discuss the effect on the fracture process of the crack tip blunting due to plasticity. Then we present the results of further analyses, which were performed with the aim of including different blade geometries in our study.

2 | THE ANALYTIC MODEL

2.1 | The wedge model

In this section, we present a 2-dimensional analytic model that describes the cutting process. A blade, consisting of a rigid elliptic wedge, is inserted in the target material, exemplified by a large elastic solid. By considering a section of the solid normal to the blade axis, we assume that an initial centred cut of length $2a$ is present in the material (Figure 2). During the evolution of the cutting process, the elliptic wedge is assumed not to move inside the cut but rather to expand. For instance, this model of the elliptic wedge could be used to describe the cutting process of an elliptic conical blade penetrating into a solid along a direction parallel to the blade axis. The shape of the elliptic wedge is expressed by

$$h(x) = \frac{h_o}{\ell}\sqrt{\ell^2 - x^2}, \tag{1}$$

where ℓ and h_o are the major and minor semiaxes, respectively. The radius of curvature at a generic point of the ellipse is given by

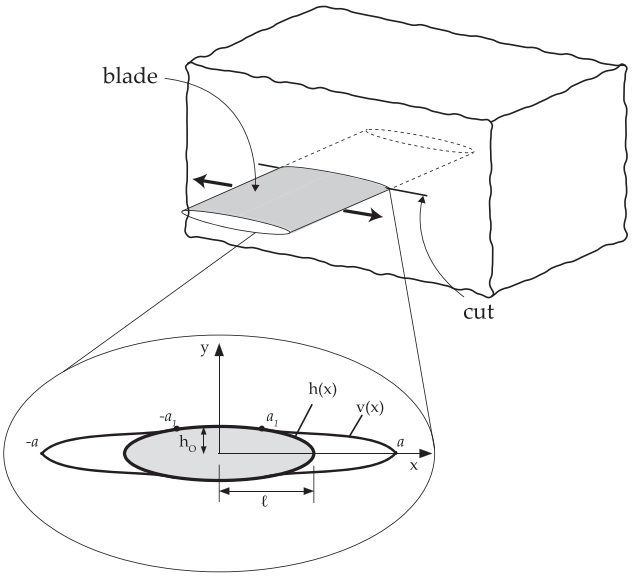

FIGURE 2 Schematic of the analytic model. An elliptic blade is inserted in a cut of length $2a$. In the enlarged figure, the vertical displacement $v(x)$ of the cut surfaces, caused by the insertion of the elliptic blade of length $\ell < a$, is also shown

$$\rho(x,h) = (h_o\ell)^2\left(\frac{x^2}{\ell^4} + \frac{h^2}{h_o^4}\right)^{3/2}, \tag{2}$$

which at the wedge tips is equal to

$$\rho(x = \pm\ell, h = 0) = \frac{h_o^2}{\ell}. \tag{3}$$

A boundary value problem may now be formulated. With reference to the Cartesian coordinate system xy of Figure 2, the cut extends along the region $|x| \le a, y = 0$. Let $v(x)$ describe the vertical displacement of the cut after separation. We suppose that the elastic solid is stress-free far away from the wedge and do not consider the effect of friction. Because of the double symmetry, only the upper-right quarter of the solid can be considered.

The wedge is assumed to be shorter or equal to the cut, ie, $\ell \le a$, and partly in contact with its surfaces. As a result, we have prescribed displacements $h(x)$ over the length $x \le a_1$, where unilateral contact conditions are assumed, that is, normal tractions must be compressive and interpenetration is not permitted. The following set of equations applies

$$v(x) = h(x), \quad \sigma_y(x) \le 0 \quad \text{for } x \le a_1. \tag{4}$$

In the adjacent region, the contact between the cut surfaces is lost, then normal stresses must be null. The following set of equations here applies

$$\sigma_y(x) = 0, \quad v(x) > h(x) \quad \text{for } a_1 < x < \ell, \tag{5}$$

$$\sigma_y(x) = 0, \quad v(x) > 0 \quad \text{for } \ell \le x < a. \tag{6}$$

Ahead of the cut, continuity and symmetry bring the displacements unconditionally to zero, while no conditions regarding permissible normal tractions can be established

$$v(x) = 0 \quad \text{for } x \ge a. \tag{7}$$

As a result of frictionless interfaces and symmetry conditions, shear stresses are null everywhere along the crack plane

$$\tau_{xy}(x) = 0 \quad \text{for } y = 0. \tag{8}$$

2.2 | Solution

The problem described by the boundary conditions (4-8) is decomposed into 2 different cases, which are solved separately. A superposition provides the solution of the overall problem.

Let us first consider the region occupied by the elliptic wedge. A well-known solution of fracture mechanics is that of a crack in an infinite plate, subjected to a uniform pressure σ_o applied to its surfaces (Figure 3A). Assuming the crack length equal to 2ℓ, in plane stress conditions, the vertical displacement is expressed as[18]

$$v(x) = \frac{2\sigma_o}{E}\sqrt{\ell^2 - x^2} \quad \text{for} \quad x \le \ell, \tag{9}$$

which is the equation of an ellipse. The equivalence with the elliptic wedge of Equation 1 is obtained if

$$\sigma_o = \frac{Eh_o}{2\ell}. \tag{10}$$

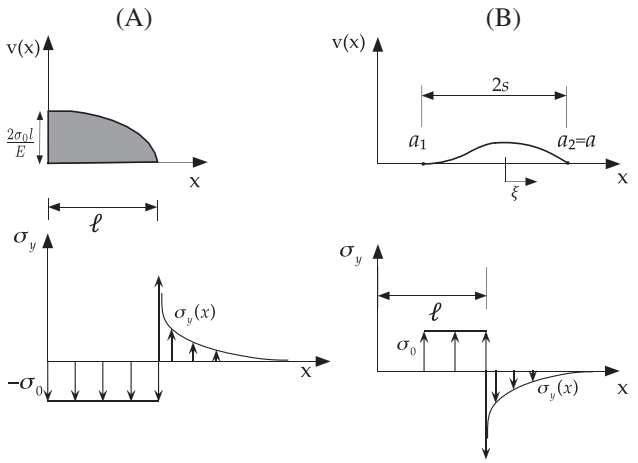

FIGURE 3 Decomposition of the solution. A, The first case shows the equivalence between the rigid elliptic wedge and a crack of length 2ℓ with an applied pressure σ_o. B, A crack of length $2s$ is considered, with prescribed stresses on its surface, to equilibrate those obtained from the previous case. Notice the discontinuity in the displacement derivative at $x = a_2 \equiv a$

Solving for the stresses, we have

$$\sigma_y(x) = \sigma_o \text{ for } x \le \ell, \tag{11a}$$

$$\sigma_y(x) = \sigma_o \left(\frac{x}{\sqrt{x^2 - \ell^2}} - 1 \right) \text{for } x > \ell. \tag{11b}$$

Comparing this solution with the conditions defined in the boundary value problem (4-8), we may notice that they are fully satisfied for the part of the wedge where contact is enforced, ie, for $x \le a_1$. On the contrary, the condition on normal stresses for the open part of the cut, ie, $a_1 \le x < a$, is not satisfied.

To equilibrate the normal stresses in the open part and obtain the correct solution to the boundary value problem, we consider a crack of length $(a_2 - a_1)$ (Figure 3B). The following tractions need to be applied to its surfaces

$$\sigma_y(x) = \sigma_o \quad \text{for } a_1 \le x < \ell, \tag{12a}$$

$$\sigma_y(x) = \sigma_o \left(1 - \frac{x}{\sqrt{x^2 - \ell^2}}\right) \quad \text{for } \ell \le x < a_2. \tag{12b}$$

As for the displacements, we prescribe that

$$v(x) = 0 \quad \text{for} \quad x > a_2 \text{ and for } x < a_1. \tag{13}$$

To find the solution to this problem, firstly, we observe that stress singularities are expected at $x = a_1$ and at $x = a_2$. We denote the corresponding stress intensity factors K_{I,a_1} and K_{I,a_2}. The unilateral contact conditions of Equation 4 exclude negative and positive stress intensity factors for the internal point a_1. In the absence of any external compressive load, an opening displacement imposed on the cut surfaces implies a positive stress intensity factor at the crack tip; therefore, we have $a_2 \equiv a$. The following conditions on the stress intensity factors shall be introduced

$$K_{\mathrm{I},a_1} = 0, \tag{14a}$$

$$K_{\mathrm{I},a_2} \ge 0. \tag{14b}$$

The general computation of the mode I stress intensity factor is performed using a weight function as follows:

$$K_{\mathrm{I}} = -\frac{1}{\sqrt{\pi s}} \int_{-s}^{s} \sigma_y(\xi) \sqrt{\frac{s + m\xi}{s - m\xi}} \mathrm{d}\xi, \tag{15}$$

where $s = (a_2 - a_1)/2$ is the half length of the crack, $\xi = x - (a_1 + a_2)/2$, $m = -1$ for the crack tip at $x = a_1$, and $m = +1$ for the crack tip at $x = a_2$. Replacing σ_y from Equations 12a and 12b, the previous integral is conveniently split into 2 parts

$$K^{(1)}_{\mathrm{I},n} = -\frac{\sigma_o}{\sqrt{\pi s}} \int_{-s}^{t} k(m,\xi)\mathrm{d}\xi = -\sigma_o \sqrt{\pi s}, \tag{16a}$$

$$K^{(2)}_{\mathrm{I},n} = \frac{\sigma_o}{\sqrt{\pi s}} \int_{t}^{s} \frac{\ell - t + \xi}{\sqrt{(\xi - t)(2\ell - t + \xi)}} k(m,\xi)\mathrm{d}\xi, \tag{16b}$$

$$K_{\mathrm{I},n} = K^{(1)}_{\mathrm{I},n} + K^{(2)}_{\mathrm{I},n}, \tag{16c}$$

where $t = \ell - (a_1 + a_2)/2$, n is equal to a_1 or a_2, and $k(m,\xi) = \sqrt{\frac{s+m\xi}{s-m\xi}}$. Introducing the normalised variables $u = \xi/s$, $\hat{t} = t/s$, and $\hat{\ell} = \ell/s$, we obtain

$$K_{\mathrm{I},n} = -\sigma_o \sqrt{\pi} + \frac{\sigma_o}{\sqrt{\pi}} \int_{\hat{t}}^{1} \frac{\hat{\ell} + u - \hat{t}}{\sqrt{(u - \hat{t})(2\hat{\ell} + u - \hat{t})}} k(m,u)\mathrm{d}u. \tag{17}$$

Taking $n = a_1$, we can substitute the previous expression in Equation 14a to determine the position of the separation point a_1

$$K_{\mathrm{I},a_1} = 0 \;\Rightarrow\; \int_{\hat{t}}^{1} \frac{\hat{\ell} + u - \hat{t}}{\sqrt{(u - \hat{t})(2\hat{\ell} + u - \hat{t})}} \sqrt{\frac{1-u}{1+u}} \mathrm{d}u = \pi. \tag{18}$$

Equation 18 provides a relation between a_1 and a_2 for any given $\hat{\ell}$, and it can be rewritten with the following recursion, which yields a single root

$$d_i = 1/\hat{\ell} = \left(\frac{1}{\pi} \int_{\hat{t}}^{1} \frac{1 + (u - \hat{t}) d_{i-1}}{(\sqrt{(u - \hat{t})(2 + (u - \hat{t}) d_{i-1})} \cdot \sqrt{\frac{1-u}{1+u}} \mathrm{d}u \right)^2, \quad \text{with} \quad d_0 = 0. \tag{19}$$

The recursion cycles are assumed to proceed until a converged result is obtained after N cycles. The value d_N is denoted d.

The stress intensity factor K_{I,a_2} is calculated taking $n = a_2 \equiv a$ in Equation 17

$$K_{\mathrm{I},a_2} = \sigma_o \sqrt{\pi} \left(\frac{1}{\pi} \int_{\hat{t}}^{1} \frac{\hat{\ell} + (u - \hat{t})}{\sqrt{(u - \hat{t})(2\hat{\ell} + u - \hat{t})}} \cdot \sqrt{\frac{1+u}{1-u}} \mathrm{d}u - 1 \right). \tag{20}$$

2.3 | Results

In Figure 4, we show the results obtained from the solution of the boundary value problem defined in Section 2.1. The dashed line is the plot of the position of the separation point a_1, as obtained from Equation 19, and normalised

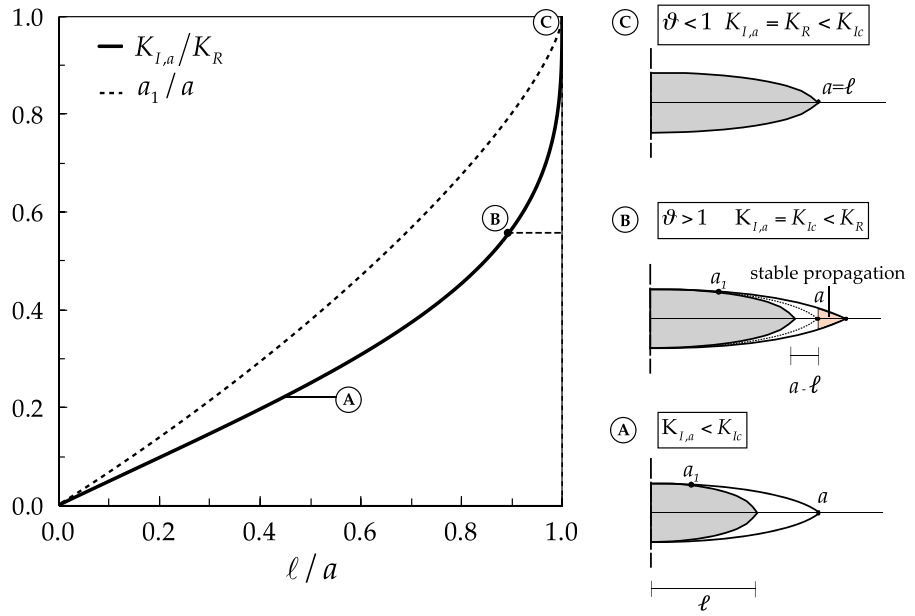

FIGURE 4 Analytic results for the elliptic wedge. The dimensionless stress intensity factor $K_{I,a}/K_R$ and the position of the separation point a_1/a are plotted as a function of the normalised length ℓ/a. The difference between a blunt wedge ($\theta > 1$) and a sharp wedge ($\theta < 1$) is illustrated [Colour figure can be viewed at wileyonlinelibrary.com]

with respect to ℓ. The continuous line is the plot of the stress intensity factor at the crack tips $K_{I,a}$. To normalise the result, we introduced K_R, the stress intensity factor that would develop if the wedge filled the entire crack, defined as

$$K_R = \sigma_o \sqrt{\pi a} = \frac{E h_o}{2} \sqrt{\frac{\pi}{a}}. \tag{21}$$

To investigate the influence of the wedge sharpness on the fracture process, a sharpness parameter is introduced, defined as the ratio between the radius of curvature ρ at the tip—see Equation 3 for an elliptic wedge—and a material-based length parameter R_c

$$R_c = \left(\frac{\pi}{2}\right)\left(\frac{K_{\mathrm{Ic}}}{E}\right)^2. \tag{22}$$

In Equation 22, R_c represents the tip radius of a crack experiencing a critical condition, K_{Ic} is the material toughness, and E is the Young modulus of the material. Making use of Equations 10 and 21, the wedge sharpness θ is equal to

$$\theta = \frac{\rho}{R_c} = \frac{8}{\pi^2}\left(\frac{K_R}{K_{\mathrm{Ic}}}\right)^2, \tag{23}$$

with $\theta < 1$ identifying a sharp and $\theta > 1$ a blunt wedge.

The graph in Figure 4 can be interpreted in the following way. With the wedge expanding inside the cut, the dimensionless stress intensity factor increases with the length ℓ/a, up to 1 when the crack is entirely filled. Different occurrences might happen, depending on the wedge sharpness. If the wedge is blunt ($\theta > 1$), $K_{\mathrm{I},a}$ increases until the limit imposed by the material toughness is attained. At this point, the crack propagates in a steady-state fashion, so that the distance between the current crack tip and the wedge tip remains constant and equal to $a - \ell$. Consequently, the wedge tip cannot reach the crack tip (point B). On the other hand, if the wedge is sharp ($\theta < 1$), the stress intensity factor $K_{\mathrm{I},a}$ peaks at a value that is smaller than the material toughness $K_{\mathrm{I},c}$ (point C). The situation of crack tip touching is now experienced by the wedge, and a certain amount of energy is required to propagate the crack. If we neglect the compressive stresses caused by the wedge, the driving force to be applied to the system is obtained as

$$F = \frac{\left(K_{\mathrm{Ic}}^2 - K_R^2\right)}{E} b, \tag{24}$$

where b is the plate thickness.

3 | NUMERICAL ANALYSES AND RESULTS

The results that we have described in the previous section offer an interesting point of view on the fracture process of cutting. Yet the need to obtain an analytic expression of the main parameters required us to simplify the geometry and the mechanical behaviour of the problem. In this section, we present the results of a series of numerical analyses that

we have performed on a finite element model. Our purpose is to validate the analytic model and explore other features that could not be included analytically. Specifically, the effect of local plasticity and of different geometries of the cutting tool.

3.1 | Fracture mechanics parameters from finite element method

The application of the finite element method (FEM) to fracture mechanics, and in particular to determine the crack tip stress and displacement fields, is well documented in the literature (see, for example, the book by Kuna[19]).

A careful design of the mesh is required. We meshed the plate using 2-dimensional elements and applied the necessary constraints to prevent rigid body motion and respect the symmetry of the problem. Convergence analyses were performed, to determine the appropriate grade of mesh refinement around the crack tip. To capture the singularities, modified elements should be used in the surroundings of the crack tip, while regular elements are suitable in the rest of the model. In a polar coordinate system (r, θ), with the origin at the crack tip, the strain singularity is proportional to $r^{-1/2}$ for an elastic material. To describe this singularity, we used 8-node, noncollapsed, isoparametric elements and shifted the midside nodes, along 2 edges converging on the tip, to 1/4 positions. In the elastic-plastic analyses, an elastic–perfectly plastic behaviour was considered. In such a case, the strain singularity is proportional to r^{-1}, and no modification of the position of the nodes is required. To model the rigid wedge, we used spring elements, with a non-linear stress-strain relationship, so that they provided stiffness only when compressed.

Initially, we performed some analyses on a model that reproduced the geometry of the analytic one to validate the results. To compute the mode I stress intensity factor from numerical analyses, one possible method is to use the displacement field. The best estimate is obtained if one uses the displacements of nodes located behind the crack tip and at a mid-range distance from it. Consequently, a linear extrapolation towards the crack tip is required. In plane stress conditions, the expression to be used is the following:

$$K_{I,a} = \lim_{r\to 0} v(r, \vartheta = \pi)\frac{E}{4}\sqrt{\frac{2\pi}{r}}. \tag{25}$$

A good approximation was obtained, both in the stress intensity factor and in the separation point, as shown in Figure 5.

3.2 | The influence of crack tip plasticity

It is well known that real materials display a certain amount of plastic deformation in the region around the crack tips, which prevents the stress singularity as predicted by elastic fracture mechanics. Moreover, if we turn our attention to the displacements, crack tip blunting is experienced, which causes the crack tip opening displacement to be different from zero.[20] According to Irwin, when plasticity occurs, the crack behaves as if it were longer than its actual size. In a first approximation, the extension of the plastic zone along the line of the crack is taken equal to

$$r_y = \frac{1}{2\pi}\left(\frac{K_{I,a}}{\sigma_{ys}}\right)^2, \tag{26}$$

where σ_{ys} is the material yield stress. In elastic fracture mechanics, the crack opening displacement is obtained as

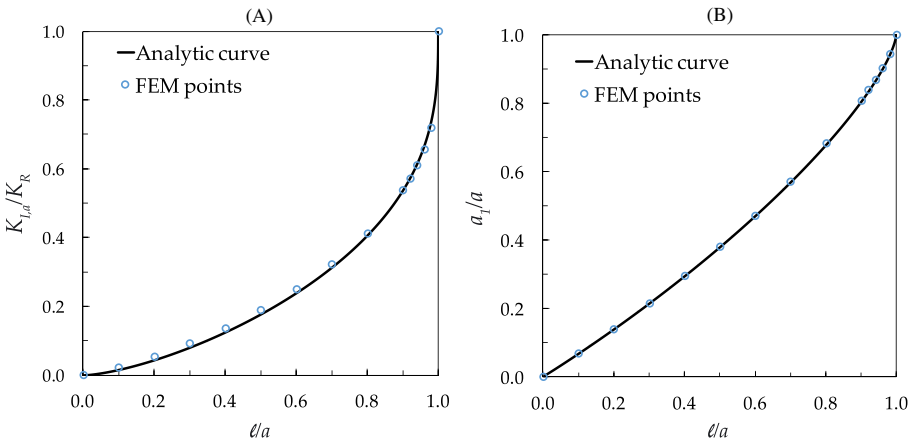

FIGURE 5 Comparison of the analytic results with finite element method (FEM) simulations. A, Plot of the stress intensity factor at the crack tip, $K_{I,a}$. Notice that the result is normalised for $K_R = \sigma_o\sqrt{\pi a}$. B, Plot of the normalised separation point a_1/a [Colour figure can be viewed at wileyonlinelibrary.com]

$$COD = 2v(x) = \frac{4\sigma_o}{E}\sqrt{a^2 - x^2}. \tag{27}$$

This goes to zero at the crack tips, ie, for $|x| = a$, but inside the plastic zone, crack tip blunting occurs, and the crack tip opening displacement is then equal to

$$CTOD = 2v(x = a) = \frac{4\sigma_o}{E}\sqrt{(a + r_y)^2 - a^2} \approx \frac{4}{\pi}\frac{{K_{I,a}}^2}{E\sigma_{ys}}. \tag{28}$$

The *CTOD* is considered as an indirect measurement of the plastic deformation occurring at the crack tips and has been proposed as part of a failure criterion in elastic-plastic fracture mechanics.[21] However, the generalisation of the *CTOD* fracture criterion beyond the limits of small-scale plasticity requires the calculation of a comparable critical parameter for the material, a task beyond the purpose of this work.

We performed some analyses on the FEM model, to evaluate the effect of local plasticity, and compared the results with those of the elastic case. For this purpose, we had to compute the *CTOD* and apply Equation 28 to get the equivalent stress intensity factor $K_{I,a}$. We should mention here that this method provides reliable results only if the plastic zone is small with respect to the crack length. To extract the *CTOD*, we used the displacements of nodes far from the crack tip, so that geometric non-linearity can be neglected,[19] and then extrapolated their values according to the following expression

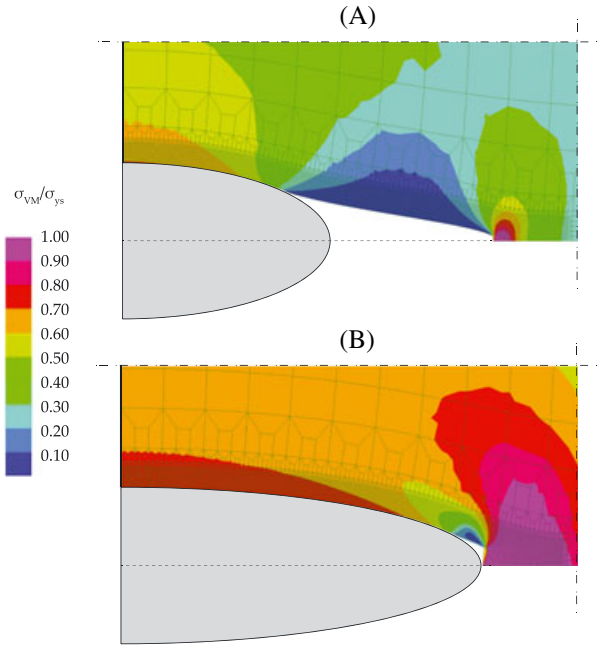

FIGURE 6 Contour plots of the combined von Mises stress σ_{VM}, normalised to the yield stress of the material σ_{ys}, with A, $\ell/a = 0.6$ and B, $\ell/a = 1$ [Colour figure can be viewed at wileyonlinelibrary.com]

$$CTOD = \lim_{r \to 0} 2v(r, \vartheta = \pi). \tag{29}$$

Figure 6 presents 2 examples of the results obtained from the finite element analyses with plasticity. The contour plots of the combined von Mises stress are displayed, considering different insertion lengths ℓ/a. The effect of the crack tip plasticity is clearer in case B, which shows the evidence of crack tip blunting. Figure 7A shows the plot of the normalised stress intensity factor for different sizes of plastic zone. The size of the plastic zone $r_{y,R}$ was defined according to Irwin's approximation, with the subscript R meaning that we have used the stress intensity factor K_R in Equation 26. A visible decrease in $K_{I,a}/K_R$ is observed when the elliptic wedge is inserted for half or more of the crack length. This result was expected. Indeed, $K_{I,a}$ is the actual stress intensity factor, that is, the one experienced at the crack tip, when the wedge is inserted for a length equal to $\ell \leq a$. Therefore, the effect of crack tip plasticity is more pronounced for $\ell/a \to 1$. The same argument explains the behaviour of the position of a_1, which is not significantly shifted by plasticity, as shown in Figure 7B.

Important deductions on the fracture process are possible. According to Irwin's approximation, Equation 26, the size of the plastic zone depends solely on the stress intensity factor and the yield stress of the material. If we introduce the fracture toughness K_{Ic}, it is possible to obtain the following expression

$$r_{y,R} = r_{yc}\left(\frac{K_R}{K_{Ic}}\right)^2, \tag{30}$$

where r_{yc} is the plastic zone corresponding to $K_{I,a} = K_{Ic}$. With this device, the graphs in Figure 7 may be used for different materials, once that 3 parameters are set: the wedge geometry, which provides K_R, the yield stress σ_{ys}, and the fracture toughness K_{Ic}.

Let us consider an example, to show how to use the graph and observe the effect of plasticity on the conditions of crack propagation. We compared the behaviour of 2 different materials, concrete and aluminium, whose mechanical properties are summarised in Table 1. Assuming, for example, that the stress intensity factor due to the wedge geometry is $K_R = 1.8K_{Ic}$, we obtained the situation illustrated in Figure 8. In the elastic material, this situation corresponds to what we have previously defined as a blunt wedge (see point B in Figure 4): $K_{Ic} < K_R$; hence, we have stable propagation of the cut when the wedge is inserted for a length $\ell \approx 0.9a$. When we consider the effect of plasticity, the behaviour is different. In the case of concrete, the plastic zone is rather small, not large enough to determine a marked difference: the wedge still behaves as blunt, although the insertion length is longer than in the elastic material. The main difference occurs for aluminium, where a larger plastic zone determines a radical change. As

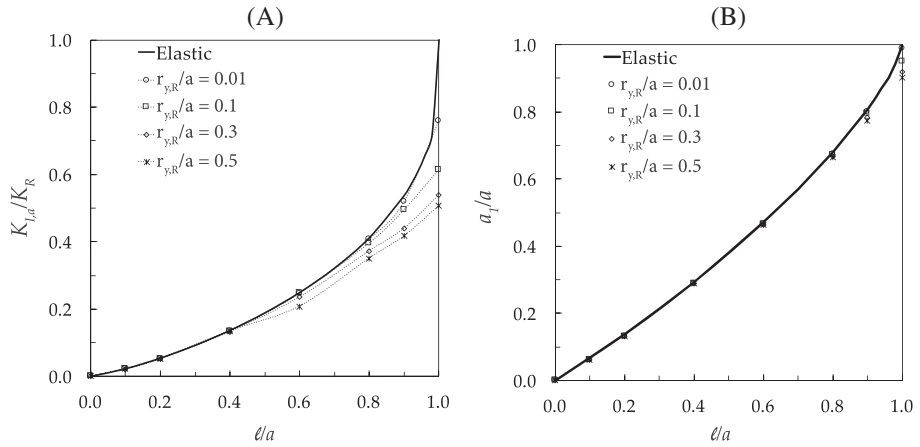

FIGURE 7 Results of finite element method simulations with plasticity. The curves were obtained considering different sizes of the plastic zone. A, Plot of the dimensionless stress intensity factor $K_{I,a}/K_R$. B, Plot of the normalised separation point a_1/a [Colour figure can be viewed at wileyonlinelibrary.com]

TABLE 1 Mechanical properties of some common materials

Material	K_{Ic}, MPa$\sqrt{\text{m}}$	σ_{ys}, MPa	r_{yc}, μm
Concrete	0.8	4	12.7
Steel	20	172	4.3
Aluminium	21	36	108.4
Titanium	55	1480	0.4

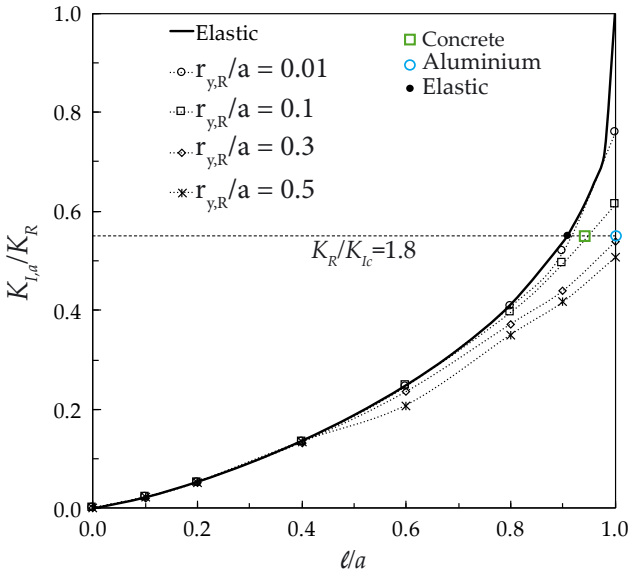

FIGURE 8 The effect of plasticity on the fracture process. Two different materials are compared with the elastic solution. The plastic zone extension is $r_{y,R}/a = 0.04$ for concrete and $r_{y,R}/a = 0.35$ for aluminium [Colour figure can be viewed at wileyonlinelibrary.com]

it can be noticed, the blue circle in Figure 8 lies on the vertical axis $\ell/a = 1$, whereas the corresponding curve stays somewhere below. In this situation, $K_{Ic} > K_R$, the wedge is to be considered sharp, implying that some force needs to be applied from the outside to propagate the cut.

3.3 | The effect of the tool geometry

A new feature we were able to investigate with the FEM analyses was the effect of different tool geometries. At this point, we chose to overcome one of the main limitations inherent to the analytic model, that is, the boundary conditions: namely, a cutting process that does not initiate from

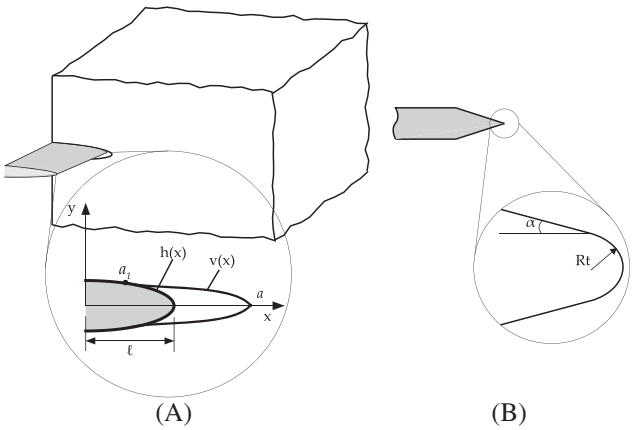

FIGURE 9 Schematic of the model used to investigate the effect of the tool geometry. A, An elliptic blade is inserted in an edge cut of length a in an elastic material. B, Blades with different features, characterised by an opening angle α and a tip radius R_t

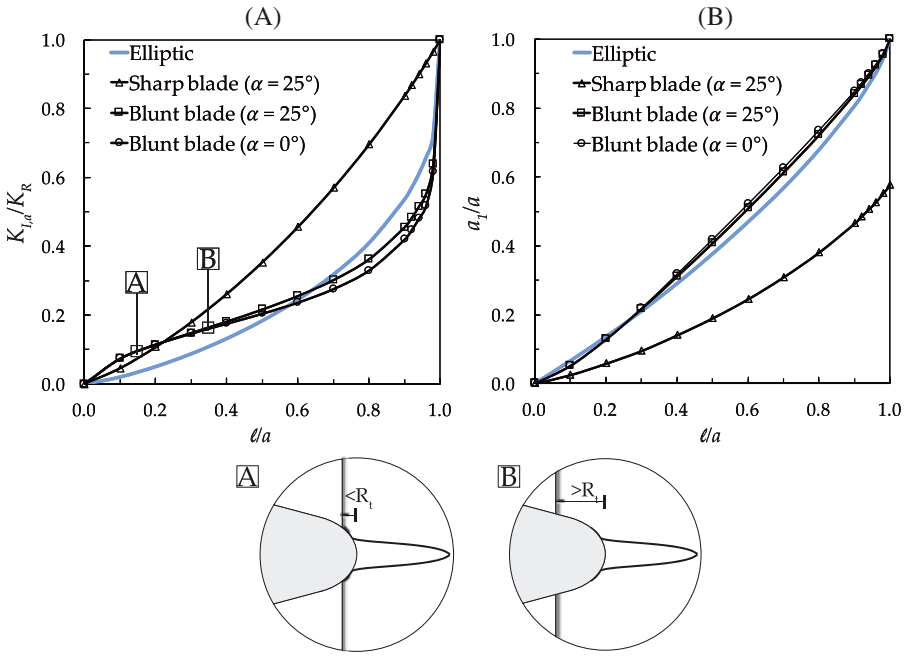

FIGURE 10 The effect of the tool geometry on the fracture process, from finite element method simulations. An edge crack model was used. A, Plot of the dimensionless stress intensity factor $K_{I,a}/K_R$. B, Plot of the normalised separation point a_1/a [Colour figure can be viewed at wileyonlinelibrary.com]

a free boundary is rather unrealistic. For this reason, we changed the model constraints to simulate an edge crack, of length a, and explored the effect of different cutting tools. An elastic behavior was considered (Figure 9A).

The tool geometry is defined by the wedge opening angle α and the wedge tip radius R_t, Figure 9B. We considered 3 different cases: a sharp blade, with an angle $\alpha = 25°$, and 2 blunt blades, one with a wedge angle $\alpha = 25°$ and the other straight ($\alpha = 0°$). Blunt blades are characterised by a nonzero value of the tip radius R_t. In commercial blades, this is often in the order of a fraction of micrometres. Our purpose was to get an insight in the effect of the tool geometry on the fracture process, with no claim of adopting real blade features. Besides, the grade of mesh refinement of our finite element model is not sufficient to capture the effect of a very small tip radius. Being the size of the elements along the crack equal to $0.002a$ (with $a = 1$ mm), we considered $R_t = 0.2$mm to be a reasonable value.

The results are gathered in Figure 10. In these plots, we used the elliptic wedge as a reference. It might be noticed that the sharpness of the blade has a remarkable influence on the cutting response, while the effect of the opening angle seems to be more limited for the cases being considered. In particular, the limit case of a perfectly sharp blade implies that a shorter insertion length is enough to cause the cut propagation, when compared to the blunt blades. In addition, Figure 10B shows that, for a given insertion length, the extension of the traction-free zone ($a_1 - a$) is larger for sharp than for blunt blades. Observing the trends in Figure 10A for the blunt blades, it should be noted that the blade shape is fully described by a circular arc during the initial penetration stage ($\ell/a \lesssim 0.2$), as shown in the enlarged figures. On the other hand, in the subsequent stage, the blade profile is composed by a circular arc and a straight segment. Another point worth to be mentioned is the fact that blunt blades have a constant radius of curvature R_t, whereas in the elliptic wedge the tip radius linearly increases with the insertion length ℓ. This might help to appreciate the differences between the curves.

4 | CONCLUDING REMARKS

The present work focuses on the steady-state conditions for indentation cutting. In the reference case of elastic behaviour of the target material, a plane boundary value problem has been studied analytically using some classical fracture mechanics parameters, and describing the cutting tool as an elliptic rigid wedge. A blade sharpness parameter has been identified as a key factor in the cutting response of the material.

We have explored the effect of plasticity, as well as of the tool geometry, by means of finite element models, where no-traction spring elements were used to simulate the unilateral contact between the material and the cutting tool. As far as plasticity is concerned, we have shown that the fracture process tends to differ from the elastic case as a

function of the relative extension of Irwin's plastic zone with respect to the crack length. The elastic modulus of the target material does not influence the response. On the other hand, the tip radius of the blade chiefly influences the attainment of a steady state of cutting. Among the cases that have been considered, it is the limit case of a perfectly acute blade that seems to yield the most severe effect, ie, a higher value of the stress intensity factor for a given insertion length. In the present work, we have not considered the effect of friction between the blade and the material, which would give rise to some resistance force to the penetration of the blade into the material. Future investigations are planned to consider such an effect. The aim will be to effectively model the characteristics of the experimental force-displacement profiles during the insertion of the cutting blade into the target material.

ORCID

M. Terzano https://orcid.org/0000-0002-3467-5079
A. Spagnoli http://orcid.org/0000-0002-0592-7003
P. Ståhle http://orcid.org/0000-0002-8067-603X

REFERENCES

1. Atkins AG. *The Science and Engineering of Cutting: The Mechanics and Processes of Separating, Scratching and Puncturing Biomaterials, Metals and Non-Metals*. Oxford: Butterworth-Heinemann/Elsevier; 2009.
2. Ernst H. Physics of metal cutting, machining of metals. *Trans ASME*. 1938;26:1-34.
3. Merchant ME. Mechanics of the metal cutting process. I. Orthogonal cutting and a type 2 chip. *J Appl Phys*. 1945;16(5):267-275.
4. Hill R. The mechanics of machining: a new approach. *J Mech Phys Solids*. 1954;3(1):47-53.
5. Atkins AG. Modelling metal cutting using modern ductile fracture mechanics: quantitative explanations for some longstanding problems. *Int J Mech Sci*. 2003;45(2):373-396.
6. Atkins AG. Toughness and cutting: a new way of simultaneously determining ductile fracture toughness and strength. *Eng Fract Mech*. 2005;72(6):849-860.
7. Williams JG. Friction and plasticity effects in wedge splitting and cutting fracture tests. *J Mater Sci*. 1998;33(22):5351-5357.
8. Williams JG, Patel Y, Blackman BRK. A fracture mechanics analysis of cutting and machining. *Eng Fract Mech*. 2010;77(2):293-308.
9. Yuan Z, Zhou M, Dong S. Effect of diamond tool sharpness on minimum cutting thickness and cutting surface integrity in ultraprecision machining. *J Mater Process Technol*. 1996;62(4):327-330.
10. Komanduri R, Chandrasekaran N, Raff LM. Effect of tool geometry in nanometric cutting: a molecular dynamics simulation approach. *Wear*. 1998;219(1):84-97.
11. Reilly G, McCormack B, Taylor D. Cutting sharpness measurement: a critical review. *J Mater Process Technol*. 2004;153-154(1-3):261-267.
12. Hill R, Lee EH, Tupper SJ. The theory of wedge indentation of ductile materials. *Proc R Soc A Math Phys Eng Sci*. 1947;188(1013):273-289.
13. Ciavarella M, Hills D, Monno G. Contact problems for a wedge with rounded apex. *Int J Mech Sci*. 1998;40(10):977-988.
14. McCarthy CT, Hussey M, Gilchrist MD. On the sharpness of straight edge blades in cutting soft solids: part I—indentation experiments. *Eng Fract Mech*. 2007;74:2205-2224.
15. McCarthy CT, Annaidh AN, Gilchrist MD. On the sharpness of straight edge blades in cutting soft solids: part II—analysis of blade geometry. *Eng Fract Mech*. 2010;77(3):437-451.
16. Shergold OA, Fleck NA. Mechanisms of deep penetration of soft solids, with application to the injection and wounding of skin. *Proc R Soc A Math Phys Eng Sci*. 2004;460(2050):3037-3058.
17. Goh SM, Charalambides MN, Williams JG. On the mechanics of wire cutting of cheese. *Eng Fract Mech*. 2005;72(6 SPEC. ISS.):931-946.
18. Broberg KB. *Cracks and Fracture*. Cambridge: Elsevier Science; 1999.
19. Kuna M. *Finite Elements in Fracture Mechanics: Theory-Numerics-Applications*, Solid Mechanics and Its Applications. New York: Springer Netherlands; 2013.
20. Broek D. *Elementary Engineering Fracture Mechanics*. New York: Springer Netherlands; 1982.
21. Wells AA. Unstable crack propagation in metals: cleavage and fast fracture. In: Proc. Crack Propag. Symp.; Cranfield, 1961:210-230.

How to cite this article: Terzano M, Spagnoli A, Ståhle P. A fracture mechanics model to study indentation cutting. *Fatigue Fract Eng Mater Struct*. 2018;1–10. https://doi.org/10.1111/ffe.12750